LAWRENCE
LIVERMORE
NATIONAL
LABORATORY

UCRL-JRNL-227892

Theory and Fluid Simulations of Boundary Plasma Fluctuations

R. H. Cohen, B. LaBombard, L. L. LoDestro, T. D. Rognlien, D. D. Ryutov, J. L. Terry, M. V. Umansky, X. Q. Xu, S. Zweben

February 8, 2007

Nuclear Fusion

Disclaimer

Theory and Fluid Simulations of Boundary Plasma Fluctuations

R H Cohen[1], B LaBombard[2], L L LoDestro[1], T D Rognlien[1], D D Ryutov[1], J L Terry[2], M V Umansky[1],X Q Xu[1], S Zweben[3]

[1] Lawrence Livermore National Laboratory, Livermore CA 94550 USA
[2] Massachusetts Institute of Technology, Cambridge, MA 02139 USA
[3] Princeton Plasma Physics Laboratory, Princeton, NJ 08540 USA

E-mail: rcohen@llnl.gov

Abstract. Theoretical and computational investigations are presented of boundary-plasma microturbulence that take into account important effects of the geometry of diverted tokamaks – in particular, the effect of x-point magnetic shear and the termination of field lines on divertor plates. We first generalize our previous "heuristic boundary condition" which describes, in a lumped model, the closure of currents in the vicinity of the x-point region to encompass three current-closure mechanisms. We then use this boundary condition to derive the dispersion relation for low-beta flute-like modes in the divertor-leg region under the combined drives of curvature, sheath impedance, and divertor tilt effects. The results indicate the possibility of strongly growing instabilities, driven by sheath boundary conditions, and localized in either the private or common flux region of the divertor leg depending on the radial tilt of divertor plates. We re-visit the issue of x-point effects on blobs, examining the transition from blobs terminated by x-point shear to blobs that extend over both the main SOL and divertor legs. We find that, for a main-SOL blob, this transition occurs without a free-acceleration period as previously thought, with x-point termination conditions applying until the blob has expanded to reach the divertor plate. We also derive propagation speeds for divertor-leg blobs. Finally, we present fluid simulations of the C-Mod tokamak from the BOUT edge fluid turbulence code, which show main-SOL blob structures with similar spatial characteristics to those observed in the experiemnt, and also simulations which illlustrate the possibility of fluctuations confined to divertor legs.

PACS numbers: 52.35.Kt,52.30.Ex,52.35.Mw,52.65.-y,52.40.Kh

1. Introduction

Turbulent transport in the boundary plasma of tokamaks play an essential role in establishing the boundary conditions for core-plasma transport and in establishing the pattern of power and particle loss to bounding material surfaces. While such transport has been the subject of theoretical, computational, and analytic studies for many years, the description of the turbulence has been heavily shaped by two major developments:

the recognition of the role of magnetic shear in the vicinity of the separatrix X-point, and the emergence of the importance of large-amplitude intermittent structures, or "blobs".

X-point magnetic shear squeezes magnetic flux tubes, mixing poloidal/toroidal and radial potential variations, thereby raising the effective radial mode number of fluctuations passing near the x point [1]. The radial wavelength of moderate-toroidal-mode-number perturbations can shrink to less than a gyroradius on passing the x-point region. Various mechanisms – resistive current flow [2], polarization [3, 4, 5], and viscosity [6] can lead to current closure in this region, thereby terminating fluctuations present on one side or the other of the x point, and isolating instabilities in the main SOL from those in the divertor leg. This current closure can be approximated as a lumped boundary condition; this was done for resistive closure in Ref. [2] , and for polarization in Ref. [3, 4, 5]. The effective boundary condition can then be used to analyze the effect of x-point shear on instabilities. This was done for curvature-driven modes in the main SOL [7], and for sheath-driven modes in the divertor leg [2].

A number of experiments (*e.g.,*, Refs. [8, 9, 10]) have observed large-amplitude, intermittent, strongly elongated (along the magnetic field) structures, or "blobs". They are of considerable importance, since they propagate radially and can be a significant transport mechanism to the main chamber walls. These can be viewed as a nonlinear state of instabilities in the SOL. A simple model was proposed in Ref. [12]; more recent treatments have introduced the braking effect of contact with external walls [11, 13], and more quantitative analyses based on the vorticity equation [13, 14].

In the past few years the interaction of the above two phenomena has come under investigation. It has been recognized that blobs (like lower-amplitude fluctuations in the edge) can be strongly impacted by the presence of X-point shear, and the effects can be analyzed using the "heuristic boundary condition" described in above. Ref. [11] derived the terminal velocity of an isolated blob in the main scrape-off layer contact with the X-point region. Recently we pointed out [15, 16] a number of further consequences of X points and wall contact (or lack thereof) for blob dynamics.

In the present paper we extend the above lines of investigation in several ways. First, we note that the X-point current-clsoure mechanisms can be combined to a generalized heuristic boundary condition (Sec. 2). We then apply (Sec. 3) the heuristic boundary condition to the analysis of low-β, flute-like, divertor-leg instabilities, under the combined influence of curvature, sheath impedance, and radial tilt of divertor plates. In Sec. 4 we gather our previously derived results on the effect of X point effects on blob propagation, and examine the reconnection of a main-SOL blob to the divertor plate as it radially propagates. We also in this section derive results for the propagation of blobs in divertor legs. Sec. 5 is devoted to numerical simulation of the above phenomena using the BOUT two-fluid code: main-SOL blobby structures and comparisons with experimental data for the C-MOD tokamak, and simulations indicating the presence of fluctuations in divertor legs uncorrelated with fluctuations in the main SOL. Sec. 6 is a discussion and summary of the results.

2. X-Point Boundary Conditions

2. X-point boundary conditions

As has been mentioned in the Introduction, in a number of cases the magnetic shearing of perturbations near the X point is so strong that it causes a complete decoupling of perturbations at two sides of the x point. In particular, perturbations in the common flux region of the divertor get decoupled from perturbations in the main SOL, and perturbations in the outer private flux region in divertor are decoupled from perturbations in the inner region. What happens to perturbations in the transition zone is that the cross-field current becomes non-negligible because of a rapid increase of a perpendicular wave number along the field line and the corresponding increase of a cross-field current. The cross-field wave number grows, roughly, as $\exp(s/L^*)$ [1], with s being the distance along the field line, and L^* being some characteristic length determined by the details of the divertor design and being of order of a few meters for most of the medium-size tokamaks [17]. So, a potential perturbation of the form $\exp(i\mathbf{k}_\perp \cdot \mathbf{r})$ imposed on the one side of the X-point decays when one moves into the X-point region because of the finite parallel plasma resistance. The situation here is similar to that of the "leaky circuit," where the voltage applied between two conductors decreases with the distance from the terminal if there is a current leak from one conductor to another.

As a rough way for describing this situation, one can impose a resistive boundary condition at a "control surface" situated at some distance from the X-point. In particular, when one deals with instabilities in the private flux region, the location of the control surfaces for the outer and inner legs are shown in Fig. .. The exact location of this surfaces is not very important if the divertor legs are long enough, so that the SOL width at the divertor plate is much less than the distance from the divertor plate to the X-point. The structure of the boundary condition at this surface is: $j_\parallel = \Sigma\delta\phi$, where Σ is some coefficient that, generally speaking, depends on the wave number and the frequency of perturbations. The form for σ depends on the assumption of the mechanism leading to the cross-field "leak."

In Ref. [18] it was noted that, when the perpendicular wave number of perturbations exceeds $\rho_i - 1$, a cross-field conductivity by electrons becomes possible. This leads to the BC of the form:

$$j_\parallel = \sigma_H \left|\mathbf{k}_\perp\right| \delta\phi \quad , \qquad \sigma_H = \omega_{pe}^2/4\pi\omega_{ce} \quad . \tag{1}$$

The parameter σ_H has the dimension of electrical conductivity and was called in Ref. [18] a "heuristic conductivity."

In Ref. [6], a closure mechanism associated with the cross-field ion shear viscosity was considered. It leads to the following BC:

$$j_\parallel = \sigma_H \left|\mathbf{k}_\perp\right| \delta\phi \left(\frac{m_e}{m_e}\right)^{1/4} \left(\left|\mathbf{k}_\perp\right| \rho_i\right)^{1/2} \quad . \tag{2}$$

[We find it convenient to express the BC in terms of the heuristic resistivity, which allows an easy comparison between various models.]

In Refs. [3, 4, 5], the closure by the ion polarization current was considered. This yields the following BC:

$$j_{\parallel} = \sigma_H \left|\mathbf{k}_{\perp}\right| \delta\phi \left(\frac{m_e}{m_e}\frac{|\omega|}{\nu_{ei}}\right)^{1/2} \tag{3}$$

The last two mechanisms are based on the assumption that the cross-field length scale of the perturbation in the sheared region remains greater than the ion gyro-radius all over the zone where the closure of the currents occurs. If, formally, the closure does not occur up to the point where the length scale becomes less than ρ_i , then the mechanism described by Eq. (1) takes over.

The BC condition for a specific set of parameters is determined by the mechanism that yields the highest current. One can qualitatively take this circumstance into account by introducing a "generalized boundary condition" that can be obtained simply by summing up Eqs. (1)-(3). The result is

$$j_{\parallel} = \sigma_H \left|\mathbf{k}_{\perp}\right| \delta\phi \left[1 + \alpha_1(k)\left(\frac{m_e}{m_e}\right)^{1/4}(k\rho_i)^{1/2} + \alpha_2(k)\left(\frac{m_e}{m_e}\frac{|\omega|}{\nu_{ei}}\right)^{1/2}\right] \tag{4}$$

The coefficients $\alpha_1, \alpha_2 < 1$ account for the aforementioned possibility that the length-scale reaches the ion gyroradius before the substantial shortening of the current by a particular mechanism occurs. The values of these coefficients depend on the specifics of the divertor geometry. For the plasma parameters chosen in Sec. 3, 4 all the mechanisms yield the same contribution, within a factor of 2-3. In order not to overload our largely conceptual analysis by the unnecessary details we use in Sec. 3, 4 simply the heuristic boundary condition (1). Possible uncertainties are taken into account by introducing the adjustment factor G in the r.h.s. of Eq. (1).

3. Divertor-Leg and Private-Flux Instabilities

The plasma in the divertor is in direct contact with the divertor plates and, therefore, may be strongly affected by the sheath boundary conditions. In the private flux region there is obviously no connection with the main SOL along magnetic-field lines. In the common flux region the connection is present but may be strongly reduced by the shear near the X-point. As noted in Refs. [19, 2, 15] these features can be used to reduce the divertor heat load by exploiting various instabilities specific to the divertor plasma so that the plasma cross-field diffusion in the divertor legs would be maximized and lead to a broadening of the wetted area. On the other hand, the possibility of confining these instabilities within divertor, without inducing additional transport in the main SOL, would eliminate any adverse effect of these instabilities on the pedestal formation and bulk plasma confinement. This approach generally favors divertors with "long legs" and can therefore improve performance of the X divertor [20].

In this paper we present an analysis of divertor-leg instabilities that consistently includes curvature, X-point shear and sheath boundary conditions (BC); we discuss the consequences for instabilities in the private flux region. We use the generic divertor

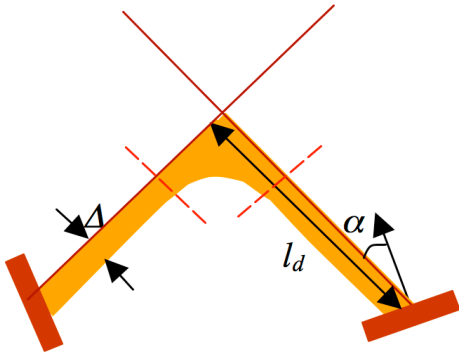

Figure 1. Schematic of the private flux region Dashed lines represent the "control planes". The major axis is to the left.

geometry shown in Fig. 1. The angle α is considered positive when the tilt of the divertor plate is as shown in Fig. 1. We assume that the distance ℓ_d from the X-point to the divertor plate is ~ 20 cm, $B_T \sim 5$ T, $B_P \sim 0.3$ T at the divertor floor, $T_e \sim 25$ eV, the plasma cross-field length-scale $\Delta \sim 1$ cm in the private-flux region at the divertor plate, and $n \sim 10^{13}$ cm^{-3}. These parameters roughly correspond to those of a high-field compact tokamak like C-Mod, although they do not reflect details of any particular tokamak. We assume also that the plasma fills the whole flux-tube connecting the inner end outer strike points, neglecting variation of the parameters along the flux tube.

We consider unstable modes satisfying $\Delta^{-1} < k_\perp < \rho_i^{-1}$, where $\rho_i = c_s/\omega_{ci}$ with $c_s = (2T_e/m)^{1/2}$. As the private flux plasma has very low beta, electrostatics is sufficient. (We can verify a posteriori that resistive ballooning is insignificant). The modes are flute-like, with $k_\parallel \ll k_\perp$. For the set of parameters mentioned above, $\rho_i \sim 0.02$ cm (deuterium). An important factor is the squeezing of the flux tubes on their way from one strike point to the other, caused by strong shear near the X point [1, 17]. A flux tube that is circular at one strike point and centered a distance Δ_0 from the separatrix ends up having a highly stretched elliptical cross-section, with ellipticity $E \approx (\ell_d/\Delta_0)^2$. Hence a perturbation with wavenumber $k_\perp$ at the outer strike point has a scale length $k_\perp^{-1}E^{-1/2} \sim k_\perp^{-1}\Delta_0/\ell_d$ near the inner strike-point. If this scale-length becomes less than ρ_i, the perturbation is "dissolved" in the ambient plasma. In this case perturbations in the two legs are disconnected and the effect of the X-point shear can be approximated by the "heuristic boundary condition" [2] on control planes situated somewhat below the X-point (dashed lines in Fig. 1). Conversely, if $\Delta_0/k_\perp\ell_d > \rho_i$, the perturbation connects the two strike points. Estimating $\Delta_0 \approx \Delta/2$, one finds that the disconnection occurs for the perturbations with $k_\perp\rho_i > \Delta/2\ell_d \sim 1/40$, *i.e.*, even for perturbations with the cross-field length-scale approaching the plasma thickness Δ. Therefore, we consider only disconnected perturbations.

We apply a sheath BC at the divertor plate, with the effects of tilt ($\sin\alpha \neq 0$) and plasma drifts included, and the heuristic BC at the control surface. We assume $T_e^{-1}\nabla_\perp T_e \gg n^{-1}\nabla_\perp n$ and neglect the latter. In the eikonal approximation, we arrive at

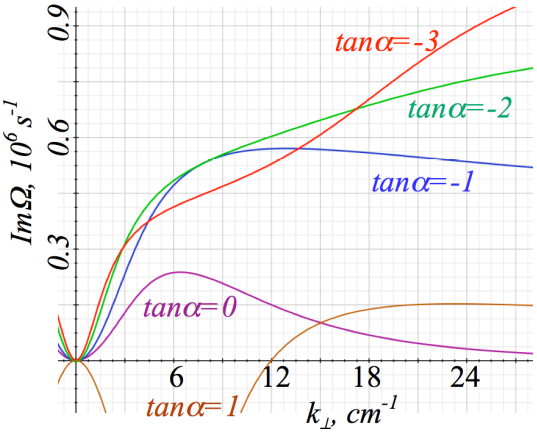

Figure 2. Growth rate versus wavenumber for the private flux region in the outer leg, for $L_\parallel = 3$ m, $R = 0.5$ m, $G = 2$, and other parameters as indicated in the text. At zero tilt, there is only a weak instability. Negative tilt makes the plasma strongly unstable.

the following dispersion relation:

$$\Omega^2 + \Omega(i\Omega_1 + \Omega_2 + i\Omega_3) - i\Gamma_1^2 - \Gamma_2^2 - \Gamma_3^2 = 0 \tag{5}$$

with

$$\Omega_1 = \frac{\omega_{ci}^2 m_i c_s}{L_\parallel k_\perp^2 T_e}, \quad \Omega_2 = \frac{\omega_{ci}}{k_\perp L_\parallel}\frac{B}{B_p}\tan\alpha, \quad \Omega_3 = \frac{B\omega_{ci}G}{B_p k_\perp L_\parallel},$$

$$\Gamma_1^2 = \frac{\hat{\Lambda}\omega_{ci}c_s}{k_\perp L_\parallel \Delta}, \quad \Gamma_2^2 = \pm\frac{T_e}{m_i L_\parallel \Delta}\tan\alpha, \quad \Gamma_3^2 = \pm\frac{T_e B}{m_i R\Delta B_p}$$

with $L_\parallel$ the distance along a field line from the divertor plate to the control surface, and the constant $\hat{\Lambda} =\sim (1/2)(1 + \ln m_e/2\pi m_i) \sim 4$. Here G is an adjustment factor of order one that enters the heuristic boundary condition [2], and R is evaluated at the strike point. The "plus" ("minus") sign corresponds to the outer (inner) leg.

The first term in the left hand side (LHS) of Eq. (5) describes plasma inertia. The last term describes curvature stabilization (destabilization) of perturbations: in the private flux region, for the outer leg, it is stabilizing, whereas for the inner leg it is de-stabilizing. The second to the last term describes the stabilizing/destabilizing effect the divertor-plate tilt. In order to have stronger turbulent broadening of the private flux region it is desirable to have $\alpha < 0 (> 0)$ in the outer (inner) leg. The Ω_3 term describes the effect of the X-point-shear boundary condition. The rest of the terms come from the sheath boundary condition (Cf. [2]). As shown in Fig. 2, the real part of the frequency at moderate k's is of the order of the growth rate, i.e., $f = \mathrm{Re}\Omega/2\pi \sim \mathrm{Im}\Omega/2\pi \sim 100$ kHz. The diffusion coefficient evaluated by a mixing length estimate is quite high, approaching 1.5 m^2/s (i.e., significantly higher than Bohm). At the non-linear stage of the instability, one can expect formation of blobs [12] moving away from the separatrix, deeper into the private flux region. This is discussed in the next section.

4. Blobs

In the past few years it has been recognized that blobs (like lower-amplitude fluctuations in the edge) can be strongly impacted by the presence of X-point shear, and the effects can be analyzed using the "heuristic boundary condition" described in Sec. 2 Ref. [11] derived the terminal velocity of an isolated blob in contact with the X-point region. Recently we pointed out [15, 16] a number of further consequences of X points and wall contact (or lack thereof) for blob dynamics. Here we collect these results, and then examine two aspects that were not explicitly treated previously: the process by which a blob loses contact with the X-point region, and the condition for resistive ballooning isolating a blob from the end walls. We then consider the implications for blob propagation in C-Mod, where some rather detailed studies of blob propagation have been performed. Finally we discuss properties of blobs that follow from the divertor-leg instabilities discussed in the preceding section.

The salient results from Refs. [15, 16] are: (1) The X points decouple blobs and blob dynamics in the main SOL and in the divertor legs. Blobs born close to the separatrix in either the main SOL or the divertor leg will be confined to that region until they have propagated out far enough that the X-point shearing is sufficiently weak. The terminal velocity of a blob confined to the main-SOL region is of order

$$\dot{R}_x \sim v_{ti} L_x \rho / GRa \tag{6}$$

where L_x is the field line connection length (half the field line length) to the X point region, a is the blob radius, ρ is the gyroradius, and G is the order-unity phenomenological constant in the X-point heuristic boundary condition. (2) Divertor leg instabilities, such as are discussed in Sec. 3, can grow into blobs localized to the divertor legs. These move slower than main-SOL-localized blobs because of contact with the divertor (see discussion below). (3) Blobs which may from birth extend all the way from the main SOL to the divertor floor, will in effect move independently in the man SOL and divertor. (4) when a blob has propagated sufficiently far from the separatrix that X-point shear is insufficient to bring the blob thickness down to the gyroradius, it ceases to be confined poloidally to one side or the other of the X-point region. (We examine below just where and how this occurs). We had argued previously that the blob would then enter a period of acceleration while simultaneously expanding along the magnetic field at thermal speed until a material surface is reached, but the discussion below indicates this period is of zero length. (5) A blob in contact with a material surface, and for which the pressure or density distribution within the blob cross section is non-symmetric, experiences a conducting-wall drive in addition to the better-known curvature drive. These blobs are the nonlinear limit of the conducting-wall temperature-gradient modes described in Ref. [21]. The terminal velocity in the case where this drive dominates over curvature drive (valid for $\Lambda a R F_a / \rho_i L_c > 1$, where $\Lambda = \hat{\Lambda} - 1/2 \sim 3$, L_c is the connection length ($\sim$ half the field-line length) and $F_a < 1$

is a measure of the degree of asymmetry of the pressure and density distributions) is

$$\dot{R}_{cw} \sim F_a \Lambda c T_{e,\mathrm{wall}}/eBa \tag{7}$$

(neglecting modifications, analagous to those discussed in the preceding section, when there is a significant tilt of the bounding surface); in the opposite limit, it is

$$\dot{R}_{\kappa} \sim (cT_e/eBa)(\rho_s L_c/Ra)(1 + T_i/T_e) \tag{8}$$

The question of how a blob, initially confined to the main SOL plasma, re-establishes connection through the divertor leg to the divertor plates, and the associated question of how far from the separatrix the X point is effective in isolating a blob has not been explicitly dealt with in the previous literature. An estimate for the critical distance from the separatrix Δ_c proceeds as follows: as noted in Ref. [1], a flux tube that is initially circular far above the X point, with radius a and distance from the separatrix Δ, is elliptically distorted to have a thickness (minor radius) $\delta R \approx a\Delta/y_D$ at a poloidal distance y_D toward the divertor, measured from the separatrix (up to the limit where the quadrupolar approximate for the poloidal field breaks down, *i.e.* up to $y_D \sim r_d$, where $r_d \sim$ minor radius is the poloidal distance over which the poloidal field projected from the quadrupolar approximation is equal to the main-SOL poloidal field); y_D is measured in the same way as ℓ_d in Fig. 1. The blob effectively terminates at the "control surface" defined by where δR becomes $\sim \rho_i$, which occurs at $y \approx a\Delta/\rho$. This increases with Δ.

One might be concerned that this point would recede toward the divertor faster than the material in the blob can catch up. However, within the context of the quadrupolar model, the toroidal distance between the position where a flux tube is circular with a specified radius r_0 and the position where it is elliptical with minor radius ρ_i is independent of the distance from the separatrix, and is just $\Delta z = (B_0/B_p')\ln(r_0/\rho_i)$, where B_0 is the toroidal field strength and B_p' is the (constant) derivative of the poloidal magnetic field with respect to distance from the X point. Hence as a blob propagates outward, this poloidal distance doesn't change. As a first approximation, one might argue that to leading order in B_p/B_t, purely transverse displacement of a flux tube consists of purely poloidal motion and so preserves the toroidal length. But this is not quite correct; transverse displacement necessarily involves some toroidal motion as well.

To estimate the effect, consider X-point geometry with x, y coordinates chosen as in Fig. 1 (whereby, along a field line, $x > y$ is in the main SOL and $y > x$ is in the divertor leg), and consider a flux tube with circular cross section of radius a_0 at position x_0, y_0 (where $x_0 \sim$ the tokamak minor radius, and $y_0 \sim$ the SOL width). This flux tube is squeezed to a radial extent $\delta x \sim \rho_i$ at position $y_f \approx y_0(a_0/\rho_i)$, $x_f = x_0 y_0/y_f$. Note that the flux tube is extended in the poloidal (y) direction here, $\delta y\, a_0^2/\rho_i$. We consider a purely transverse displacement of the flux tube which is purely in the poloidal plane at x_0, y_0; for a radial displacement ξ_{0y}, there is a poloidal displacement $\xi_{0x} \sim -\xi_{0y} B_y/B_x = \xi_{0y} y_0/x_0$, and by construction zero toroidal displacement. We look for the point on the displaced field line which is reached by a purely transverse (to $\mathbf{B}$) displacement from the point x_f, y_f, z_f, That is, $\boldsymbol{\xi}_f \cdot \mathbf{B} = 0$, from which it

follows that $\xi_{fz} = (B_p'/B_0)(x_f\xi_{fx} - y_f\xi_{fy})$. Just as the shear results in the flux tube being elongated in the y direction, the displacement ξ_{yf} is enhanced over the main-SOL displacement ξ_{y0} by the same factor $\sim a_0/\rho_i$. Hence we find, approximately, $\xi_{fz} \sim -\xi_{y0}B_p'y_F^2/B_0y_0\ \xi_{y0}(B_p/B_0)a/\rho$. Hence, as a blob moves outward with velocity $\dot{R}$, there must be a toroidal flow (approximately equal to the toroidal flow) of magnitude $v_\parallel \sim \dot{R}(B_p/B_t)(a/\rho_i)$ in order to preserve Δz and so stay up with the receding control surface. For typical parameters $(B_p/B_t)(a/\rho_i) \sim 1$; the required parallel flow velocity is of the same order as the blob radial expansion velocity, which must be sub-sonic in order for the derived expressions to apply. So, the blob can keep up with the receding control surface; the X-point boundary condition will continue to apply until the control surface reaches the divertor plate. The limit of applicability of the X-point boundary condition is then simply given by $\Delta_c \approx \rho\ell_d/a$. A blob propagating past this point will transition from a terminal velocity set by X-point shear to a terminal velocity set by contact with the divertor plate.

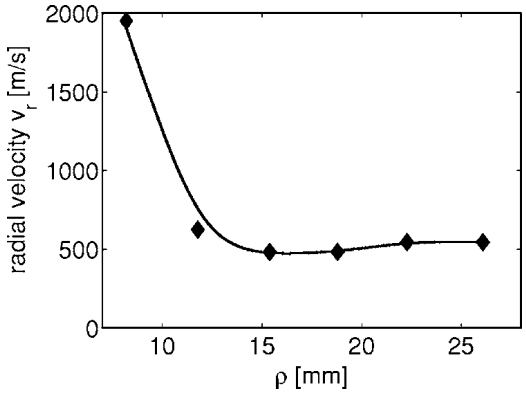

Figure 3. Blob propagation speed in C-Mod, from Ref. [9].

Another useful criterion that can be extracted from Ref. [16] is the criterion that resistive ballooning isolate a blob from material endwalls. Eqs. (42) and (43) of Ref. [16] are coupled partial differential equations for the evolution of the normal and geodesic component of displacement for a blob derived in the approximation of resistive MHD, and are of the form:

$$C_1\ddot{\xi}_g + \frac{B^2}{c^2}\frac{\partial}{\partial s}\left[C_{gg}\left(\frac{B}{B_p}\xi_g\right) + C_{gn}\left(B_pR\xi_n\right)\right] + S_g = 0 \tag{9}$$

and

$$C_1\ddot{\xi}_n + \frac{B^2}{c^2}\frac{\partial}{\partial s}\left[C_{nn}\left(\frac{B}{B_p}\xi_n\right) + C_{ng}\left(B_pR\xi_g\right)\right] + S_n = 0 \tag{10}$$

where $C_1 = \int \rho dS$, $C_{jg} = (\int \sigma dS)D_{jg}B_p/B^2$, $C_{jn} = (\int \sigma dS)D_{nj}/BB_pR$, and $S_j = [2(\nabla B)_n/B]\int pdS$ for $j = g, n$, $\int dS$ denotes an integral over the cross section of the blob, $D_{ij} = \langle x_ix_j\rangle - \langle x_i\rangle\langle x_j\rangle$, σ is ithe electrical conductivity, and the $\langle\ \rangle$ denotes a σ-weighted average over the blob cross section. The resistive ballooning limit prevails

when the parallel derivative terms in these equations are negligible compared to the remaining terms, from which we obtain the following criterion:

$$\dot{R} \ll \dot{R}_b = \beta c^2 L_c^2/\pi a^2 \sigma R \tag{11}$$

where σ is the parallel conductivity.

We now consider application of these considerations to C-Mod. Ref. [9] contains a plot of blob velocity versus radius for a representative discharge, reproduced here as Fig. 3. A striking feature is that, apart from the large velocity shown at the smallest radius (which the authors regard as an instrumental artifact), the velocity is nearly constant, and does not show much structure. One is then led to ask how to reconcile this with theoretical predictions of blob speeds that depend on what surfaces the blob contacts and whether it passes close to the X point. Appeals to ballooning don't help: blobs in C-Mod are observed to have radii $\sim$ 1 cm (see e.g. Fig. 9 of ref. [9]); hence taking $B = 5$T, $R = 0.9$m, the ballooning criterion, Eq. (11), becomes $\dot{R} \ll \dot{R}_b \sim 94$ m/s$\times(n/5 \times 10^{13}\text{cm}^{-3})(L_c/5\text{ m})^2(1\,\text{cm}/a)^2(T/20\text{ ev})^{-1/2}$, which, for the observed blob velocity from Fig. 3 and typical C-Mod parameters, is not satisfied except possibly very close to the separatrix where the field lines become very long. So indeed we must consider where blobs end. The criterion that they "end" at the X-point control surface rather than at the divertor plate, $\Delta < \Delta_c = \rho\ell_d/a$, becomes $\Delta < 0.4\text{cm} \times(T_{e,\text{wall}}/10\text{eV})(\ell_d/20\text{ cm})$. (Because of the shape of the C-Mod divertor, ℓ_d varies appreciably). Thus only the left-most data point in Fig. 3 is possibly subject to the X-point boundary condition. For all other data points the blobs are in contact with either the horizontal leg of the divertor structure or the antenna limiter. For C-Mod conditions with the asymmetry parameter $F_a \sim 1$, the criterion for dominance of conducting-wall drive for blobs is strongly satisifed; hence for all blobs that end on a wall (limiter or divertor), we estimate $\dot{R} = \dot{R}_{cw} \sim 640$ m/s $\times(T_{e,\text{wall}}/10$ ev$)(1$ cm$/a)F_a$. This is of the right order of magnitude and could plausibly be consistent with a constant blob velocity if the asymmetry parameter F_a compensates for a decrease in blob temperature as it propagates. For a blob that terminates in the X-point shearing region (possibly, marginally, the left-most data point), we obtain $\dot{R} = \dot{R}_x \sim 4400$m/s $\times(T/20$ eV$)(2/G)(1\text{cm}/a)$; a blob that just misses termination by X-point shearing would instead terminate on the vertical surface of the C-Mod divertor structure, which would also have an elevated propagation speed because of the tilt of the surface relative to poloidal field lines. The change in velocity between the first and second data points in Fig. 3 is plausibly the slowing-down of the blob as it transitions from ending in the X-point region or the vertical divertor surface to terminating on the horizontal divertor or limiter surfaces.

We return to the discussion of divertor-leg blobs, noted in Sec. 3 If the electron temperature in the blob is uniform, the drive is associated with the curvature and the tilt of the divertor plates. The contact with the conducting divertor plate partially reduces the polarization field and gives rise to a constant-velocity motion. The x-point "heuristic boundary condition" turns out to be high resistance compared to the

sheath, and so is effectively insulating. This leads to the estimate for the blob velocity, $\dot{R}_{dl} = (\rho_i^2 c_s/a^2)[(L_\parallel/R) \pm (B/B_p)\tan\alpha]$, where + (-) corresponds to the inner(outer) divertor leg in the private flux region, and opposite for the common flux. If the tilt term dominates over the curvature term by O(1), blob motion is strong enough to strongly affect transport; the ion parallel transit time is longer than the blob propagation time over the SOL width Δ even for blobs with size Δ for the parameters of Sec. 3 If the broadening is sufficient to result in reconnection of the inner and outer strike points in the private flux region, and there is enough tilt with favorable signs at both plates, further broadening is possible. Finally, we note a preliminary report of an observation on the MAST spherical tokamak suggestive of the existence of a divertor-leg blob; fast camera observations in visible light during ELM-free periods following an L-H transition appear to sho continued presence of field-line-following filaments in the divertor region but an absence of filaments in the main SOL [22].

5. BOUT Simulations

We present in this section simulations of edge turbulence using the BOUT code [23], that illustrate the concepts discussed in the preceding sections. Specifically we address simulations of blobby turbulence in C-Mod, and present simulations showing divertor-leg turbulence uncorrelated with main-SOL turbulence for DIII-D.

We present first simulations of edge turbulence for the MIT Alcator C-Mod tokamak. Edge plasma in C-Mod is relatively dense ($n_i \sim 0.5\times10^{20}$ m^{-3}) and cold ($T_e \sim 30$ eV) that makes it a particularly good choice for application of the collisional Braginski-based plasma model. A particular C-Mod shot 1031204007, t=740 ms is modeled with the magnetic geometry based on an EFIT reconstruction. For the profiles of background plasma density N_{i0} and temperature T_{e0} a fit is constructed to match the scanning Langmuir probe measurements at the outer midplane location, with no poloidal variation. In divertor legs the radial profile is taken symmetric with respect to the separatrix, see Fig. (4). The background ion temperature, T_{i0}, is taken identical to T_{e0}, and no background equilibrium flow and no equilibrium electric potential is used. In the calculation the toroidally average components of fluctuating fields are subtracted out, thus keeping the toroidally average components unchanged.

Two simulation cases are considered, one treating the magnetic equilibrium as a lower single-null (LSN), and the other extending the domain to include the secondary X-point resulting in an unbalanced double-null (UDN).This C-Mod discharge is nominally considered a LSN, and the first simulation is done for that geometry.

As usual, the simulation is initiated with a small seed perturbation, which evolves through linear instability to a saturated turbulent state, see Fig. (5). The amplitudes of calculated N_i fluctuations are quite high: more than 50% at the separatrix and more than 100% further out, see Fig. (5). That is by a factor 2-3 larger than the experimentally measured fluctuations of the ion saturation current normalized to the mean value of the ion saturation current see Fig. (6), that can serve as an estimate of

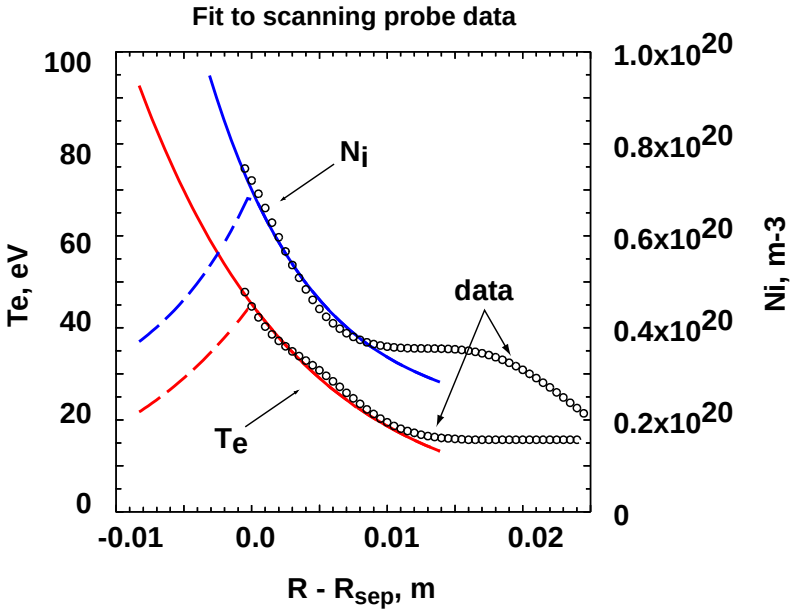

Figure 4. Background plasma profiles for C-Mod simulations

RMS$(N_i)/\langle N_i \rangle$ in the experiment.

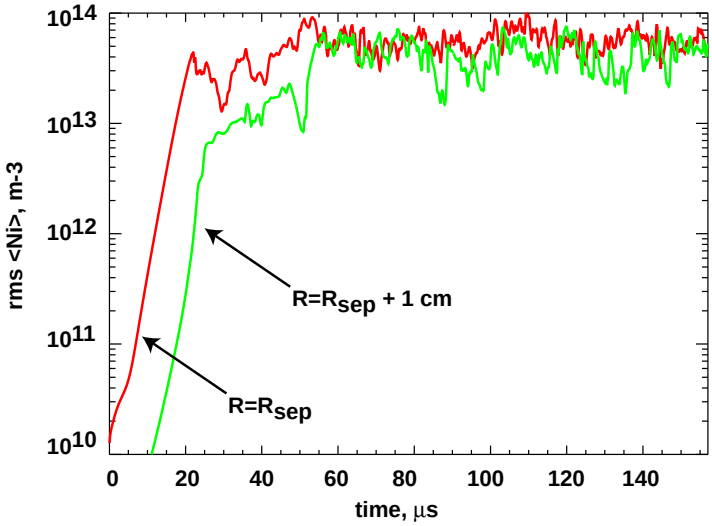

Figure 5. Growth and saturation of fluctutations C-Mod simulations

The evolution of turbulent plasma is followed for 500 μs, spanning many dozens of eddy turn-over times. The appearance of turbulent eddies is qualitatively similar to that typically observed in the experiment with the fast cameras.To make a quantitative comparison with the experiment a statistical analysis is performed yielding basic parameters such as the auto-correlation time, τ, and auto-correlation lengths in the radial, L_{rad},and poloidal,L_{pol}, directions. The value of L_{pol} is found to be in the range of typical experimental values, 0.5-1.0 cm, while L_{rad} is smaller than experimental values

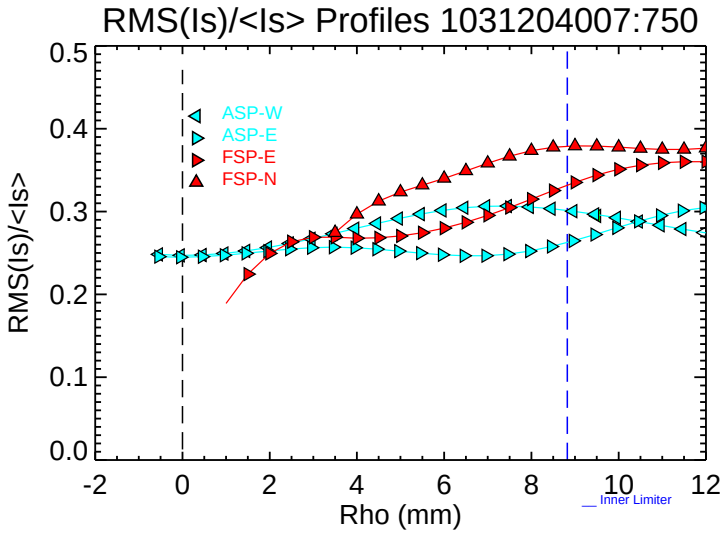

Figure 6. Fluctuations of the saturation current from scanning probe in C-Mod

0.5-1.5 cm. However the radial domain size for the LSN case is just 2 cm, constrained by the location of the secondary separatrix, which suggests that the outer boundary condition (zero fluctuation amplitude) may be affecting the solution.This LSN domain limitation is overcome by running the same case as a UDN, thereby allowing access to the more distant radial plasma region.Comparison of the two cases is shown in Fig. (7) where the UDN case yields more radially extended turbulent structures than the LSN case. That is confirmed by Fig. (8) where L_{rad} and L_{pol} are plotted vs. the poloidal and radial coordinates respectively.The corresponding range of experimental correlations lengths averaged over all radii are shown by the shaded areas. One can see in Fig. (8) thatL_{pol} is quite similar for the two cases, as expected,while L_{rad} is considerably larger for the UDN case. Comparison of the correlation time (to 1/2 of the autocorrelation peak) is less satisfactory. The BOUT values for both cases is about 2 μs, whereas C-Mod measurements indicate a value about 5 times larger. Reasons for this difference are being investigated.

In a separate series of BOUT simulations a study of plasma turbulence in divertor leg region is conducted. The basic magnetic geometry is based on a DIII-D magnetic reconstruction. The background plasma is modeled using a set of simulated toroidally-symmetric background plasma profiles that qualitatively and quantitatively approximate the equilibrium state of edge plasma as known from experimental data. In saturated turbulence fluctuations exist not only at outer midplane but in divertor legs as well, see Fig. (9). However the leg turbulence appears to be uncoupled from the upstream turbulence as shown in the cross-correlation analysis. The cross-correlation function is defined as follows:

$$C(\tilde{\phi},\tilde{\phi}) = \frac{<\tilde{\phi}(r_0,\theta,\zeta+\Delta\zeta,t+\tau)\tilde{\phi}(r_0,\theta_{ref},\zeta,t)>_{\zeta,t}}{<|\tilde{\phi}(r_0,\theta_{ref},\zeta,t)|^2>_{\zeta,t}} \tag{12}$$

Here r_0 is the radial index of the chosen flux surface, ζ is the toroidal grid index, and θ

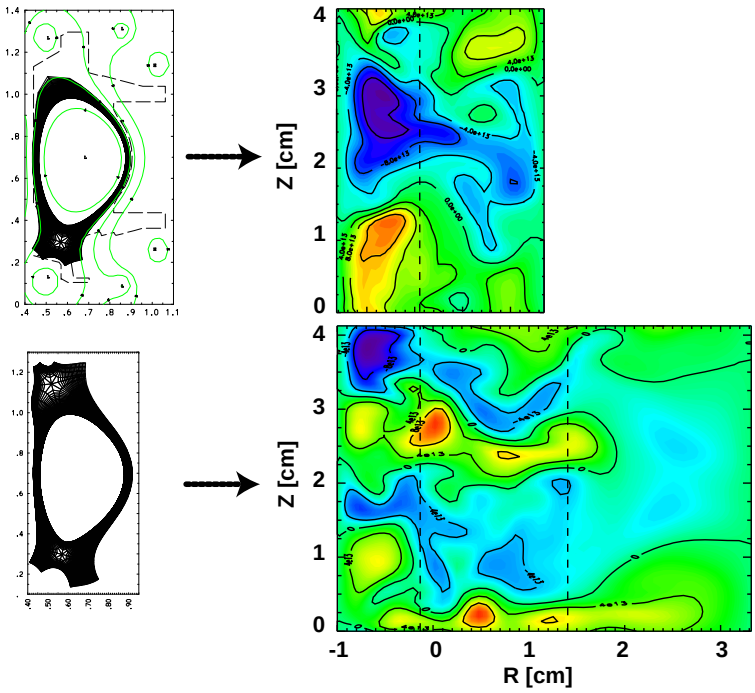

Figure 7. Fluctuations of density at outer midplane for single-null and double-null BOUT runs for C-Mod

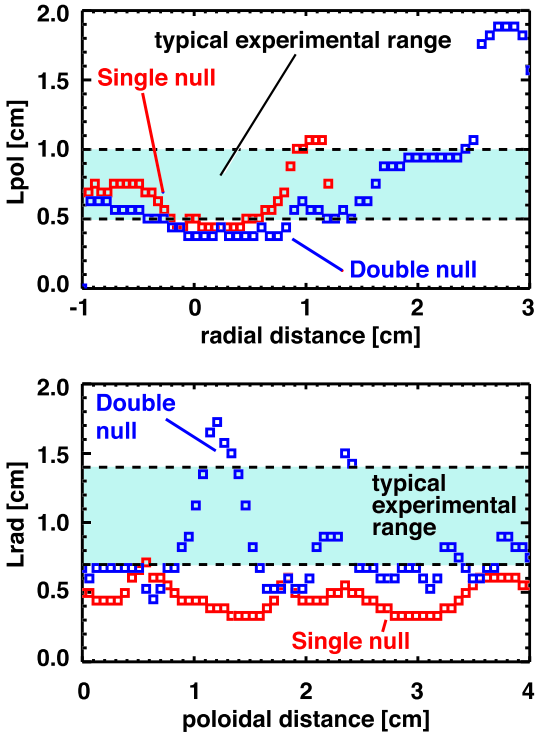

Figure 8. Correlation lengths for fluctuating density at outer midplane for single-null and double-null BOUT runs for C-Mod

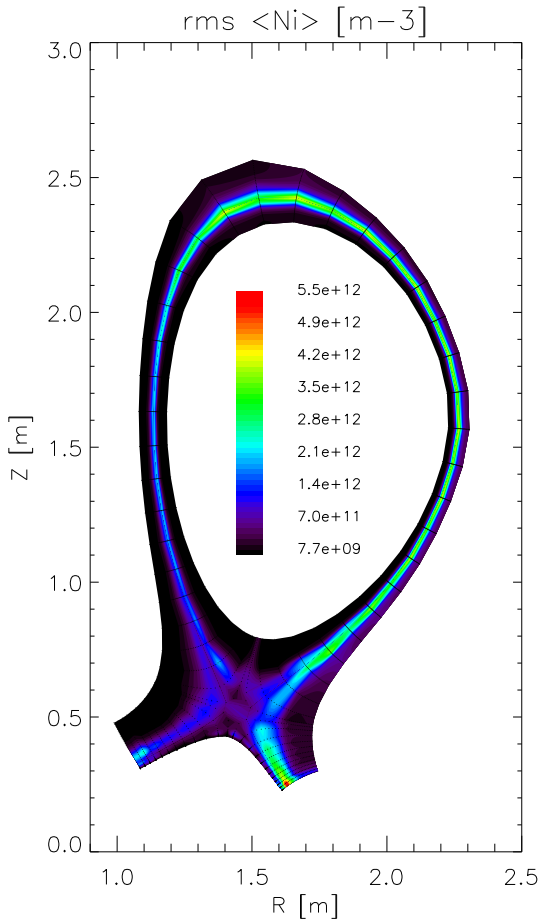

Figure 9. Distribution of rms $\langle N_i \rangle$ fluctuations in divertor leg turbulence simulations

is the poloidal index. Also, τ is the time lag, θ_{ref} is the reference poloidal index.

If the reference location is taken at the outer mid-plane then large values of the cross-correlation function correspond to locations between the lower x-point and the upper virtual x-point, see Fig. (10,A). If, however, the reference location is in the outer leg then large values of the cross-correlation function correspond to locations within the leg itself, see Fig. (10,B). This analysis shows that turbulence upstream and turbulence in the legs are uncoupled. We attribute this decorrelation to the strong shearing of magnetic field near the X-point discussed in preceding sections. It is noteworthy that decorrelated fluctuations are observed in both the linear (not shown) and nonlinear (shown) phases; hence we can attribute the divertor-leg turbulence to instabilities in the divertor leg, as discussed in Sec. 3.

6. Conclusion

From the studies presented here, we can draw the following conclusions: (1) The "heuristic boundary condition" previously developed to describe resistive closure of currents resulting from X-point shear is straightforwardly extended to simultaneously

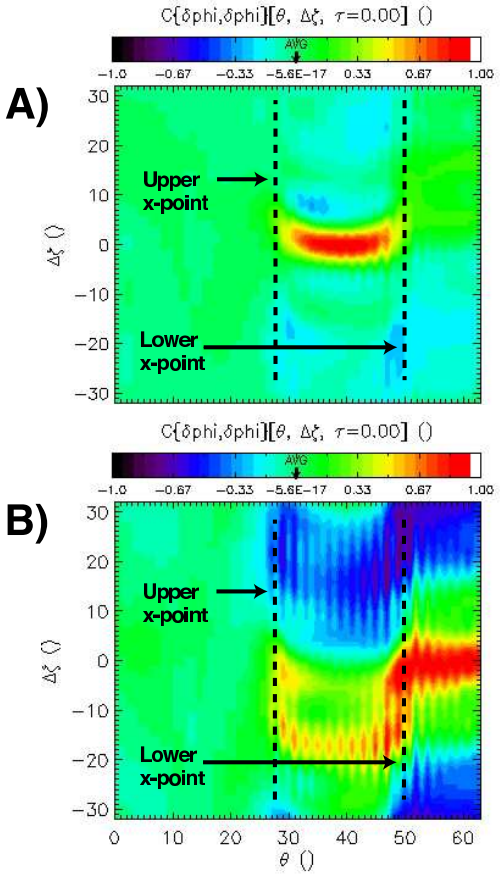

Figure 10. Cross-correlation of fluctuations in divertor leg turbulence simulations: (A) reference location at outer midplane, and (B) reference location in outer divertor leg

include polarization and viscous (as well as resistive) channels for current closure. (2) Curvature- and sheath-driven instabilities can exist in the private- as well as common-flux regions of divertor legs, isolated from the main SOL; these offer the possibility of broadening the SOL without impacting the main plasma. Divertor-plate tilt can significantly increase the growth rate. Nonlinearly these can develop into divertor-leg blobs; (3) X-point effects can isolate blobs in the main SOL from divertor legs, and non-symmetric blobs in contact with material surfaces can be dominated by sheath-impedance drive. As a main-SOL blob propagates outward, the region where X-point current closure occurs (the location of the "control surface") recedes down the divertor leg, but the propagating blob maintains contact with this region, and so propagates as a speed determined by X-point termination, until the control surface reaches a material surface. The blob propagation rate then transitions to the (lower) speed determined by contact with material walls. These results are consistent with the magnitude and relative constancy of C-Mod blob velocities reported in Ref. [9]. The X-point effects would be expected to have an impact only at the left-most data point in Fig. 3. (1) Analytic

results are qualitatively confirmed by BOUT fluid simulations. Simulations of C-MOD find blob-like structures with amplitudes and spatial correlation lengths comparable to those observed experimentally. BOUT simulations also provide evidence of instability and fluctuations in divertor legs that is incorrelated with activity in the main SOL.

Acknowledgment

This work was performed for the U.S. Department of Energy under contracts W7405-ENG-48 at U.C. LLNL and DE-AC02-76CHO3073 at PPPL, and Cooperative Agreement DE-FC02-99-ER54512 at MIT.

7. APPENDIX: Basic equations for divertor-leg instabilities

We assume that unperturbed plasma parameters do not vary along the field lines. Because of the toroidal symmetry of the unperturbed plasma, this means that the variation occurs only in the direction normal to the flux surfaces. To avoid excessively long equations, we assume that the only quantity that varies in the normal direction is the electron temperature T_e. This assumption can also be justified by the observation that the radial scale-length of T_e in the vicinity of the separatrix is usually shorter than that of the plasma density and ion temperature; also, as it turns out in the subsequent analysis, the instability drive associated with the electron temperature gradient contains a significant numerical multiplier $\sim 3-4$.

Figure 11. Simplified geometry for perturbation analysis.

Perturbations that are most unstable have a ballooning nature, with a slow variation along the field lines; in a number of cases they become essentially pure flute perturbations. For strong magnetic shear near the X-point, the perturbations in the inner and outer divertor legs are uncoupled form each other; similarly, if we consider the common flux region, we assume that perturbations are decoupled from the main SOL [1]. As shown in Ref. [2] and Sec. 2 of this paper, the presence of the X-point is folded into the analysis by introducing a boundary condition set on some "control" surface situated somewhat below the X-point. In this way, we come to the simplified geometry shown in Fig. 11. In this geometry, our earlier assumption that the unperturbed plasma parameters are constant along the field lines means that these parameters vary only in the x direction, so that the perturbations can be represented as $f(x)\exp(-i\omega t + kK_y y + iK_z z)$. Following Refs. [24, 25], we represent the two-dimensional (2D) vector $\mathbf{K}$ in the form:

$$K_y = K_y + q \quad , \qquad K_z = k_z \quad , \tag{A-1}$$

with k_y defined as

$$k_y = -k_z B_z / B_y \tag{A-2}$$

In other words, the perturbation becomes $f(x)\exp(iqy)\exp(-i\omega t + i\mathbf{k}\cdot\mathbf{r}$, with the 2D vector $\mathbf{k}$ being perpendicular to the magnetic field. The factor $\exp(iqy)$ describes (a slow) variation of perturbations along the field line, whereas the factor $\exp(i\mathbf{k}\cdot\mathbf{r})$ does not vary along the field line due to condition $\mathbf{k}\cdot\mathbf{B} = 0$, Eq. (A-2).

We assume that the poloidal magnetic field in Fig. 11 is directed towards the divertor plate, and that the toroidal component is directed towards the viewer. In other words, we assume that $B_y \equiv -B_p < 0$, and that $B_z \equiv B_t > 0$, with both

$$B_p > 0, B_t > 0. \tag{A-3}$$

We will be using the eikonal approximation, assuming that perturbation length-scale in the x direction is much less than the thickness Δ of the SOL plasma. We will also assume that the x-component of the wave number is small compared to k, i.e, $k_x \ll k$. This assumption is based on the results of the earlier works [2, 24, 25], which showed that usually the fastest-growing perturbations are of this type. The other natural assumption is that the popoidal (y) component of the magnetic field is small compared to the toroidal component: this is certainly true in a divertor with not very long legs, where the poloidal distance from the plate to the X point is significantly smaller than the plasma radius a. We will retain only the lowest-order terms in the parameters

$$k_x/k \ll 1 \quad , \qquad B_p/B_t \ll 1 \quad . \tag{A-4}$$

The second of these inequalities, when combined with condition (A-2), shows also that

$$k_z \ll k_y \quad . \tag{A-5}$$

As the plasma is in contact with the equipotential surface of the divertor plate, the variation of the electron temperature leads to the variation of the unperturbed plasma potential (as the sheath potential scales as Te [26]), and, accordingly, to the $\mathbf{E}\times\mathbf{B}$ drift in the unperturbed state. The drift causes the Doppler shift of the perturbation frequency in the (local) plasma rest-frame from Ω to

$$\Omega = \omega - \mathbf{k}\cdot\mathbf{v}_D \quad . \tag{A-6}$$

One can check *a posteriori* that the frequency shift caused by the parallel plasma flow is negligible because of the smallness of q.

The instability that we find has an e-folding time much shorter than the ion transit time from the control surface to the divertor plate. Therefore, the ion thermal spread is unimportant; it is also unimportant whether the ion mean free path is shorter or longer than the connection length $L_\parallel$ between the control surface and the divertor plane: the ions enter the problem just via their cross-field inertia. With regard to electrons, we assume that their collision frequency is higher than the growth rate. Under such conditions, the momentum equation can be written as:

$$-\Omega^2 m_i n\xi = -\nabla\delta p + frac\delta\mathbf{j}_\perp \times \mathbf{B}c \tag{A-7}$$

Here ξ is the displacement vector of a plasma element, related to the velocity perturbation by:

$$\delta\mathbf{v} = -i\Omega\xi \quad . \tag{A-8}$$

The pressure perturbation in Eq. (A-6) can be found from the electron thermal balance equation, which yields:

$$\delta p = -nT_e'\xi_x \quad . \tag{A-9}$$

We have used the fact that the perturbations are essentially divergence-free and that the only unperturbed quantity that depends on x is T_e. The prime here and below means differentiation with respect to x.

One can find the perpendicular current perturbation from Eq. (A-7):

$$\delta\mathbf{j}_\perp = \frac{c}{B^2}\left\{-\Omega^2 m_i n\left[\mathbf{B}\times\xi\right] + \left[\mathbf{B}\times\nabla\delta p\right]\right\} \tag{A-10}$$

To find the perturbation of the parallel current, one has to take the divergence of Eq. (A-10) and use the current-continuity equation, which yields:

$$\frac{B_p}{B_t}q\delta j_\parallel = -\nabla\cdot\delta\mathbf{j}_\perp = -\frac{ic\Omega^2 m_i n}{B^2}\mathbf{k}\cdot\left[\mathbf{B}\times\xi\right] + \frac{2ic\delta p}{B^3}\mathbf{k}\cdot\left[\mathbf{B}\times\nabla B\right] \tag{A-11}$$

Here we have taken into account the fact that, at the edge, the magnetic field is close to the vacuum field and, therefore, $|\nabla\times\mathbf{B}| \ll |\nabla B|$. The last term in Eq. (A-11) describes the curvature drive. Note also that the current continuity equation shows that $|\delta j_\parallel| \gg |\delta\mathbf{j}_\perp|$ (because of the large parallel wavelength of perturbations).

Using inequalities (A-4), (A-5), one finds, to the lowest order,

$$\frac{B_p}{B_t}q\delta j_\parallel = -\frac{ik_y c\Omega^2 m_i n\xi_x}{B_t} + \frac{2ick_y\delta p)(\nabla B)_x}{B_t^2} \tag{A-12}$$

The divertor legs typically form a 45-degree angle with the horizontal plane; as $\nabla B \approx -\mathbf{e}_R B_t/R$, where $\mathbf{e}_R$ is the unit vector in the direction of the major radius R, one has $(\nabla B)_x \approx -B_t/2^{1/2}R$. Using Eq. (A-4), one finally obtains:

$$\frac{B_p}{B_t}q\delta j_\parallel = -ik_y nc\xi_x\left(\frac{\Omega^2 m_i}{B_t} + \frac{w^{1/2}T_e'}{B_t R}\right) \tag{A-13}$$

In the case where the plasma is limited at both ends by non-conducting plates (so that at these surfaces $\delta j_\parallel = 0$), and displacement ξ_x is constant along the field line, this equation yields a dispersion relation for the flute instability, $\Omega^2 = -2^{1/2}T_e'$. In our case, however, the limiting surfaces are conducting, and the situation becomes more complex.

Consider now the parallel structure of perturbations. To do that, we use Maxwell equations and the Ohms law:

$$\nabla\times\delta\mathbf{B} = \frac{4\pi}{c}\delta\mathbf{j} \quad , \tag{A-14}$$

$$\nabla\times\delta\mathbf{E} = \frac{i\Omega}{c}\delta\mathbf{B} \quad , \tag{A-15}$$

$$\delta\mathbf{E} = i\Omega\frac{\xi\times\mathbf{B}}{c} + \eta\mathbf{b}\left(\mathbf{b}\cdot\mathbf{j}\right) \quad , \tag{A-16}$$

where $\mathbf{b} = \mathbf{B}/B$, and η is the parallel resistivity: based on the observation that , we retained only the parallel component of the current in the Ohms law. From Eqs. (A-14) and (A-16) one finds:

$$\delta\mathbf{E} = i\Omega\frac{\xi\times\mathbf{B}}{c} + \frac{\eta c\mathbf{b}}{4\pi}\left(\mathbf{b}\cdot\nabla\times\delta\mathbf{B}\right) \quad . \tag{A-17}$$

Substituting this result into Eq. (A-15), one obtains:

$$\delta B_x = -iB_p q\xi_x - iD_M k_y^2 \delta B_x/\Omega \tag{A-18}$$

where

$$D_M = \eta c^2/4\pi) \tag{A-19}$$

is the magnetic diffusivity. In other words,

$$\delta B_x = \frac{-iB_p q\xi_x}{1 + i\frac{D_m k_y^2}{\Omega}} \quad . \tag{A-20}$$

Using

$$ik\delta B_x = 4\pi\delta j_\parallel/c \tag{A-21}$$

and Eq. (A-10) we then find:

$$\Omega^2 = \frac{q^2 v_A^2 B_p^2}{B^2\left(1 + i\frac{D_m k_y^2}{\Omega}\right)} - \frac{2^{1/2}T_e'}{Rm_i} \quad . \tag{A-22}$$

We have used here inequalities (A-4) and (A-5). We have also assumed that, in the Ohms law, the parallel electron inertia can be neglected. This requires that the wave-number be smaller than ω_{pe}/c (note that in Ref. [25] this condition is written "upside-down").

When considered as an equation for q, equation (A-22) has two roots, $q_\pm$:

$$q_\pm = \pm q_0 \quad ; \qquad q_0 \equiv \frac{B_t}{B_p v_A}\left[\left(1 + i\frac{D_m k_y^2}{\Omega}\right)\left(\Omega^2 + \frac{2^{1/2}T_e'}{Rm_i}\right)\right] \quad . \tag{A-23}$$

This shows that the spatial structure of the perturbation in the poloidal direction is:

$$\xi_x = A\exp(iq_+ y) + B\exp(iq_- y) = A\exp(iq_0 y) + B\exp(-iq_0 y)) \tag{A-24}$$

where A and B are arbitrary constants. By imposing boundary conditions at the divertor plate and the control surface, and imposing the solvability condition, one can eliminate A and B and obtain the linear dispersion relation.

For the case of perfect line-tying at both ends, for which $q = \pi/\ell_d$, where

$$\ell_d = L_\parallel(B_p/B_t) \tag{A-25}$$

is the distance between the divertor plate and control surface (Fig. 1), Eq. (A-22) describes various regimes of a curvature-driven instability. In particular, if the plasma is perfectly conducting, we recover a standard ballooning instability for sufficiently small magnetic field (sufficiently high plasma β); at higher field (lower β), the instability is stabilized. If, on the other hand, the resistivity is high enough, the first term is significantly reduced (D_M is large), and the instability is recovered even at low betas: this is the resistive-ballooning mode. One can write down the corresponding criteria and see that, for the case of the C-Mod private flux region, β is too small to make the system unstable for perfect line tying. However, we will see below that accounting for more realistic boundary conditions at the divertor plate and control surface makes the system strongly unstable.

The boundary conditions can be cast in the form of conditions on the current flowing through the two limiting surfaces. For the solution of the form (A-21), the expressions for the parallel and perpendicular currents, to significant leading order in the small parameters B_p/B_t, k_z/k_y andk_x/k_y is (see Eqs. (A-4) and (A-5)):

$$\delta j_\parallel = -\frac{Bk_y}{Bq_0}\left(\frac{cm_i n\Omega^2}{B_p}+\frac{2^{1/2}cnT_e'}{RB_p}\right)\left[A\exp(iq_0y)-B\exp(-iq_0y)\right] \quad \text{(A-26)}$$

$$\delta\mathbf{j}_\perp = \frac{c\Omega B_t}{B^2k_y}\left(\Omega m_i n\mathbf{k}+\frac{inT_e'k_y}{\Omega B_t}\right)\left[A\exp(iq_0y)+B\exp(-iq_0y)\right] \quad . \quad \text{(A-27)}$$

The component of the plasma current normal to the end surface is (also to the lowest required order in small parameters):

$$\begin{aligned}\delta j_n|_{y=0} =& \cos\alpha\frac{B_p}{B_t}\delta j_\parallel+\sin\alpha\,(\delta\mathbf{j}_\perp)_x\\ =& -\frac{cnk_y\cos\alpha}{q_0B_t}\left(m_i\Omega^2+\frac{2^{1/2}T_e'}{R}\right)(A-B)\\ &+\frac{ick_ynT_e'\sin\alpha}{B_t}(A+B)\end{aligned} \quad \text{(A-28)}$$

$$\begin{aligned}\delta j_n|_{y=\ell_d} =& \frac{B_p}{B_t}\delta j_\parallel+(\delta\mathbf{j}_\perp)_y-\frac{cnk_y}{q_0B_t}\left(m_i\Omega^2+\frac{2^{1/2}T_e'}{R}\right)\times\\ &\left[A\exp(iq_0\ell_d)-B\exp(-iq_0\ell_d)\right]\end{aligned} \quad \text{(A-29)}$$

We assume that the length of the divertor leg is not too small, namely that $k_y\ell_d > B_t/B_p, \tan\alpha$.

We now match these currents to the currents flowing through the sheath (at $y=0$) and the current flowing to the X-point region (at $y=\ell_d$). To find these currents, we have to find the potential perturbations near these surfaces. Proceeding as in Ref. [25], we find that

$$\delta\phi = \frac{\Omega B_t}{ck_y}(A+B) \quad \text{(A-30)}$$

near the lower boundary and

$$\delta\phi = \frac{\Omega B_t}{ck_y}\left(A\exp(iq_0\ell_d)+B\exp(-iq_0\ell_d)\right) \quad \text{(A-31)}$$

near the upper boundary.

Using the boundary conditions relating the currents and potential perturbations, one can obtain the dispersion relation. At the lower boundary ($y=0$) we have from the sheath CVC (Cf. Eq. (33) of Ref. [25]):

$$\delta j_n|_{y=0} = -en(A+B)\left\{u\frac{B_p}{B_t}\cos\alpha\left[\left(\Lambda+\frac{1}{2}\right)\frac{T_e'}{T_e}+\frac{e\Omega B_t}{cT_ek_y}\right]+i\Omega\sin\alpha\right\} \quad \text{(A-32)}$$

The parameter Λ is the logarithm of the ratio of electron thermal velocity to the ion thermal velocity and is typically $\sim 3-3.5$. So, there is a significant numerical factor

in front of T_e'. As mentioned at the beginning of the Appendix, this makes the T_e' drive more important than the drive associated with, say, T_i'. From Eqs. (A-28) and (A-32), we obtain the following equation:

$$\frac{ck_y\cos\alpha}{q_0B_t}\left(m_i\Omega^2+\frac{2^{1/2}T_e'}{R}\right)(A-B)= \\ -e(A+B)\left\{u\frac{B_p}{B_t}\cos\alpha\left[\left(\Lambda+\frac{1}{2}\right)\frac{T_e'}{T_e}+\frac{e\Omega B_t}{cT_ek_y}\right]+i\Omega\sin\alpha \right. \\ \left. +\frac{ick_yT_e'\sin\alpha}{eB_t}\right\} \tag{A-33}$$

At the control surface ($y=\ell_d$), we use the "heuristic" boundary condition (see Sec. 2) which can be represented as

$$\delta j_n=\frac{B_p}{B_t}\left|k_y\right|\sigma_H\delta\phi \tag{A-34}$$

or, accounting for Eqs. (A-29) and (A-31),

$$\frac{ck_yn}{q_0B_p}\left(m_i\Omega^2+\frac{2^{1/2}T_e'}{R}\right)\left(A\exp(iq_0\ell_d)-B\exp(-iq_0\ell_d)\right) \\ =\frac{\left|k_y\right|\sigma_H\Omega B_t}{ck_y}\left(A\exp(iq_0\ell_d)+B\exp(-iq_0\ell_d)\right) \tag{A-35}$$

From the solubility condition of the set (A-33), (A-35), one can obtain a dispersion relation which covers, in a unified manner, a number of effects that have been considered previously in a piecemeal manner: the drive, associated with the temperature gradient and sheath BC, the flute instability in the presence of current leaks to the end surfaces, the role of the boundary condition at the control surface, the effect of a tilt of the divertor plate, and possible finite-beta modes. It covers also effect of resistive ballooning.

We concentrate here on the case of a low-β plasma. We first derive a simplified dispersion relation for this case by taking the limit of $v_A\to\infty$ and then formulate applicability conditions for such an approximation.

In the limit of a large Alfven velocity, one has

$$q_0\ell_d\ll 1 \quad . \tag{A-36}$$

In this case, it is convenient to introduce, instead of A and B, the coefficients a and b, according to:

$$a=\frac{A-B}{q_0} \quad , \qquad b=(A+B)\ell_d \quad , \tag{A-37}$$

One then has, for small q_0:

$$\frac{A\exp(iq_0\ell_d)-B\exp(-iq_0\ell_d)}{q_0}\approx a+b \quad ;$$

$$A\exp(iq_0\ell_d)+B\exp(-iq_0\ell_d)\approx b/\ell_d \quad , \tag{A-38}$$

so that Eqs. (A-33) and (A-35) are reduced to:

$$\frac{ck_y\cos\alpha}{B_t}\left(m_i\Omega^2+\frac{2^{1/2}T_e'}{R}\right)a\ell_d = -eb\left\{u\frac{B_p}{B_t}\cos\alpha\left[\left(\Lambda+\frac{1}{2}\right)\frac{T_e'}{T_e}+\frac{e\Omega B_t}{cT_ek_y}\right]+i\Omega\sin\alpha + \frac{ick_yT_e'\sin\alpha}{eB_t}\right\} \tag{A-39}$$

and

$$\frac{ck_yn}{B_p}\left(m_i\Omega^2+\frac{2^{1/2}T_e'}{R}\right)a\ell_d = b\left[\frac{|k_y|\,\sigma_H\Omega B_t}{ck_y}-\frac{ck_yn}{B_p}\left(m_i\Omega^2+\frac{2^{1/2}T_e'}{R}\right)\ell_d\right] \quad , \tag{A-40}$$

wherefrom dispersion relation () of the main body of the paper immediately follows.

We formulate now conditions under which the flute approximation (A-36) holds. As we are interested in modes whose growth rate is comparable to or greater than the growth rate of a curvature-driven mode, i.e., $|\Omega|^2 > T_e'/Rm_i$, one can rewrite the condition (A-36) as:

$$|q_0|\,\ell_d \approx \frac{B_t\ell_d\,|\Omega|}{B_pv_A}\left|1+i\frac{D_Mk_y^2}{\Omega}\right|^{1/2} \ll 1 \quad . \tag{A-41}$$

If the plasma electrical conductivity is high, so that the second term under the square root is small, the validity of the flute approximation becomes

$$\frac{B_T\ell_d\,|\Omega|}{B_pv_A} \ll 1 \tag{A-42}$$

[Note that in the opposite limiting case, there may exist unstable modes localized near the divertor plate; these modes have been considered in Ref. [25]. The general dispersion relation based on Eqs. (A-33), (A-35) allows one to consider various intermediate cases.]

If the electrical conductivity is low, so that

$$D_Mk_y^2 \gg |\Omega| \quad , \tag{A-43}$$

the applicability condition of the flute approximation becomes more stringent:

$$\frac{B_t\ell_d}{B_pv_A}\left(|\Omega|\,D_Mk_y^2\right) \ll 1 \quad . \tag{A-44}$$

If this condition breaks down, the unstable modes localized near the divertor plates by the effect of resistive ballooning may appear.

References

[1] Farina D, Pozzoli R, Ryutov D D 1993 *Nucl. Fusion* **33** 1315
[2] Ryutov D D, Cohen R H 2004 *Contrib. Plasma Phys.* **44** 168
[3] Russell D A, D'Ippolito D, Myra J R, Nevins M and Xu X Q 2004 *Phys. Rev. Lett.* **93** 265001
[4] Myra J R and D'Ippolito D A 2005 *Phys. Plasmas* **12** 92511
[5] Myra J R, Russell D A and D'Ippolito D A 2005 *Phys. Plasmas* **12** 92511

[6] Ryutov D D, Cohen R H and Helander P 2001 *Plasma Phys. and Controlled Fusion* **43** 1399
[7] Myra J R, D'Ippolito D A, Xu X Q and Cohen R H 2000 *Phys. Plasmas* **7** 2290
[8] Terry J L, Zweben S J, Hallatschek K, LaBobmard B, Maqueda R J, Bai B, Boswell C J, Greenwald M, Kopon D, Nevins W M, Pitcher C S, Rogers B N, Stotler D P and Xu X Q 2003 *Phys. Plasmas* **10** 1739
[9] Grulke G, Terry J.L, LaBobmbard B and Zweben S J 2006 *Phys. Plasmas* **13** 012306.
[10] Zweben S J, Macquedda R J, Terry J L, Munsat T, Myra J R, D'Ippolito D, Russell D A, Krommes J A, LeBlanc B, Stolzfus-Dueck T, Stotler D P, Williams K M, Bush C E, Maingi R, Grulke O, Sabbagh S A and White A E 2006 *Phys. Plasmas* **13** 056114
[11] Krasheninnikov S I, Ryutov D D and Yu G 2004 *J Plasma and Fusion Research* **6** 139
[12] Krasheninnikov S I 2001 *Phys. Lett.* **A 283** 368
[13] Garcia O E, Bian N H and Fundamenski W 2006 *Phys. Plamas* **13** 082309.
[14] D'Ippolito D A, Myra J R and Krasheninnikov S I 2002 *Phys. Plasmas* **9** 222.
[15] Cohen R.H, Ryutov D D 2006 *Contrib. Plasma Phys.* **46** 678
[16] Ryutov D D 2006 *Phys. Plasmas* **13** 122307
[17] Cohen R H, Ryutov D D 1996 *Contrib. Plasma Phys.* **36** 161
[18] Ryutov D D and Cohen R H 2004 *Contrib. Plasma Phys.* **44** 168
[19] Cohen R H and Ryutov D D 1997 *Nucl. Fusion* **37** 621
[20] Kotschenreuther M 2006 *private communication*
[21] Berk H L, Ryutov D D and Tsidulko Yu A, Phys. Fluids **B3** (1991) 1346, and Berk H L, Cohen R H, Ryutov D D, Tsidulko Yu A and Xu X Q 1993 Nucl. Fusion bf 33 263
[22] Counsell G 2006 *private communication*
[23] Xu X Q, Cohen R H, Rognlien T D and Myra J R 2000 *Phys. Plasmas* **7** 1951
[24] Farina D, Pozzoli R and Ryutov D 1993 *Plasma Phys. Contr. Fusion* **35** 1271
[25] Cohen R H and Ryutov D D 2005 *Plasma Phys. Contr. Fusion* **47** 1187.
[26] Stangeby P 2000 *The Plasma Boundary of Magnetic-Fusion Devices* (Inst. of Physics Publishing, Bristol and Philadelphia)

This work was performed under the auspices of the U.S. Department of Energy by University of California, Lawrence Livermore National Laboratory under Contract W-7405-Eng-48.